Precipitate/matrix incompatibilities related to the {111}$_{Al}$ Ω plates in an Al-Cu-Mg-Ag alloy

M.R. Gazizov[a,*], A.O. Boev[b], C.D. Marioara[c], R. Holmestad[d], D.A. Aksyonov[b], M.Yu. Gazizova[a], R.O. Kaibyshev[a]

[a] Belgorod State University, 308015 Belgorod, Russia
[b] Center for Energy Science and Technology, Skolkovo Institute of Science and Technology, 121205 Moscow, Russia
[c] Materials and Nanotechnology, SINTEF Industry, N-7465 Trondheim, Norway
[d] Department of Physics, Norwegian University of Science and Technology (NTNU), N-7491 Trondheim, Norway

* Corresponding author: gazizov@bsu.edu.ru

Abstract

The atomic structure of Ω plates forming on {111}$_{Al}$ planes in an Al-Cu-Mg-Ag alloy has been investigated by Z-contrast atomic-resolution scanning transmission electron microscopy imaging and *ab initio* density functional theory calculations. Ω plates with different thicknesses have been studied in two peak-aged conditions: 150 °C for 24 h and 190 °C for 1.5 h. Volumetric and structural incompatibilities as unrelaxed misfit strains and shear components, respectively, between the Ω plates involving orthorhombic θ-phase fragments and Al matrix were found to be in the plates with thicknesses from 0 to 2.5 c_θ (a normal direction to {111}$_{Al}$). Two types of shear components: [-101]$_{Al}$ // [0-10]$_\theta$ (τ_I) and [1-21]$_{Al}$ // [100]$_\theta$ (τ_{II}) related to precipitate/matrix structural incompatibilities have been predicted by calculations. The shear components τ_I and τ_{II} have been found to be energetically favorable in the plates with different thicknesses. Comparing τ_I and τ_{II} absolute values in supercells involving the plates with different thicknesses, 2 c_θ thick plates have a shear component close to zero. All the plates analyzed have precipitate/matrix volumetric incompatibilities with Al matrix as misfit strains along [111]$_{Al}$ // [001]$_\theta$, which distribute non-uniformly across the plate thickness. Large misfit strains concentrate at the broad plate interfaces, i.e. in Ag$_2$Cu and Cu$_i$ layers, and cause a prohibitively high barrier to thickening of the Ω precipitates.

Keywords: metals and alloys; precipitation; crystal structure; transmission electron microscopy, TEM; computer simulations

1. Introduction

Al-Cu-Mg-Ag alloys exhibit high specific strength, good fracture toughness and fatigue fracture in addition to superior creep resistances at elevated temperatures. This is attributed to the

uniformly distributed disperse Ω-phase forming during aging [1–10]. The Ω-phase is a $\{111\}_{Al}$ plate-shaped precipitate having a sandwich-like structure consisting of a core and broad interfaces [11–13]. Monoclinic [5], hexagonal [6,14] and orthorhombic structures [4,15,16] have been proposed for the Ω-phase core, but the later has been the most widely accepted [7,11,15,17]. Despite the variety of all the Ω-phase core structures suggested, it is quite similar to the equilibrium θ-phase (I4/mcm) having the stoichiometric composition of Al_2Cu with the epitaxial relationship $\{111\}_{Al}//(001)_\theta$, $<110>_{Al} // <010>_\theta$ and $<211>_{Al} // <100>_\theta$ [11,17,18].

The structure and chemistry of the Ω phase have been studied by high-resolution transmission electron microscopy (TEM) [4,6,11,15,19], atom probe tomography [20–23] and X-ray energy dispersive spectroscopy [24,25], but only a combination of direct experimental observations with scanning TEM (STEM) and ab initio calculations using density functional theory (DFT) enabled to establish its energetically favorable atomic configuration [7,13,16]. This structure is multilayered, composing, from the Al matrix side to the precipitate, of Ag atoms in a hexagonal configuration (Ag atom arrangement similar to Al in the respective $\{111\}_{Al}$ layer substituted), Mg atoms lying in the center of these hexagons yielding the stoichiometric composition of Ag_2Mg, and then a Cu-enriched (Cu_i) layer connected to the orthorhombic θ-phase lattice [7,11,13,16,23].

The edge interfaces of the hexagonal Ω plates are known to be predominantly free from Mg and Ag segregations in comparison with the broad plate interfaces [23], which can have coherent or semi-coherent structures depending on the plate thickness [3,11]. The semi-coherent edge interfaces were associated with misfit strain caused by volumetric incompatibility between the precipitate and matrix lattices [26]. This misfit is 9.3 % estimated on the basis of precipitate and matrix lattice parameters alone [15,21,27]. With the Ω plate thickening, the misfit-compensating dislocations (MCDs) as a Frank partial $\vec{b}$=a/3[111]$_{Al}$ at the semi-coherent edge interfaces with an average spacing of 2.5 or 3 c_θ ([111]$_{Al}$ // [001]$_\theta$ normal to the broad plane surfaces of Ω plates containing orthorhombic θ lattice) [3,11]. The very thin Ω plates were expected to behave as an elastically constrained thin film, while the elastic properties of the thick plate should be more closely approach to those of bulk precipitate structures [11]. Hutchinson et al. [11] also suggested that appearance of the MCDs may change the strain field normal to the broad interfaces for the whole Ω precipitate from vacancy (tension) to interstitial (compression) types depending on the plate thickness.

Kang et al. [7] also measured misfit strain for the Ω plates with the thickness up to 2 c_θ in atomic-resolution STEM images. These results were compared with the DFT supercells including infinite {111}$_{Al}$ plates of the Ω-phase with different elements (Cu, Mg and Ag) occupying the specific atomic sites at the broad interfaces. The misfit strain was shown to be about 0, +5, 0, -5, and 0 % for the Ω plates with thicknesses of 0, 0.5, 1, 1.5, and 2 c_θ, respectively.

It is also interesting to note that Aaronson et al. [28] and Nie et al. [29] suggested that the formation of the plate-like precipitates such as Ω (Al_2Cu) in Al-Cu-Mg-Ag alloys and T1 (Al_2CuLi) in Al-Cu-Li alloys often are associated with a significant shear component at the broad interfaces. It was also considered that strain accommodation plays an important role to control both nucleation and growth of these plate-like precipitates. In our recent work [26], the hybrid Ω precipitates (HP) having the thickness of about 0.5 c_θ and composing of orthorhombic (θ-type) and hexagonal (η-type) phase fragments were shown to predominantly form in an Al-Cu-Mg-Ag alloy peak-aged at 150 °C for 24 h and 190 °C for 1.5 h. As a result of strain accommodation due to structural precipitate/matrix incompatibility, the phase transformation (θ→η) of a part of the Ω plate becomes energetically favorable due to internal shift along [-101]$_{Al}$//[0-10]$_\theta$, while another part keeps the θ configuration. This eliminates structural incompatibility between hybrid precipitates and the Al matrix. Moreover, there are volumetric incompatibilities between the hybrid /non-hybrid precipitate with different thicknesses and the Al matrix causing misfit strains in [111]$_{Al}$//[001]$_\theta$ [3,11,26].

Structural and volumetric incompatibilities causing strain field distribution around the precipitate plates are known to play a significant role in ledge nucleation and their propagation during thickening of plate-shaped precipitates [3,11]. To improve the additional contribution to strengthening of the alloys after aging [1,2,30], it may help to better understand dislocation interaction mechanisms with these strained precipitates. A matching phenomenon of the {111}$_{Al}$ Ω plates embedded in the Al matrix, as well as the stress relaxation mechanisms for these complex precipitate structures with different thicknesses, are still poorly understood in Al-Cu-Mg-Ag alloys. Thus, knowledge regarding these incompatibilities is essential to understand their role in determining the precipitate evolution and high heat resistance of Al-Cu-Mg-Ag alloys.

In the present work, we have studied the Ω plates with thicknesses up to 2.5 c_θ. We used atomic resolution annular dark field (ADF)-STEM to verify previous bulk Ω phase structure observations [7,13]. We have analyzed the appearance of a misfit-compensating dislocation at the

edge interfaces of the {111}$_{Al}$ plates with different thicknesses for the reference to estimate compatibility between the Ω plate internal structure and stacking layers in the Al matrix. Obtained results were applied to construct supercells for *ab* initio calculations and assess the Ω precipitate energetics. DFT calculations helped to analyze volumetric and structural incompatibilities between the Al matrix and Ω plates with different thicknesses, parameterize these incompatibilities and identify energetically favorable shear component directions for better understanding this phenomenon in an Al-Cu-Mg-Ag alloy.

2. Experimental procedure

2.1. Sample preparation

An aluminum alloy with nominal chemical composition Al-4.5Cu-0.56Mg-0.77Ag-0.42Mn-0.12Ti-0.05V-0.02Fe (in wt. %) was prepared using a direct-chill, semi-continuous casting process. The chemical composition of the alloy was measured using a Foundry Master UVR optical emission spectrometer. The high amount of Mn was added to form $Al_{12}(Mn,Fe)_3Si$ and $Al_{20}Cu_2Mn_3$ dispersoids after homogenization to suppress recrystallization [1].

Initially, the alloy was homogenized at 500°C for 24 h followed by cooling in a furnace. Further, it was extruded at ~400°C with a ratio of ~2.6 and hot-rolled with a reduction of ~60 %. 20 mm thick plates were obtained to cut rectangular ~20×20×3 mm samples with a wire electric discharge machine. These samples were then heat treated at 510°C for 1 hour, quenched in water and immediately aged at 150 °C and 190 °C for different times (up to 200 h).

2.2. Mechanical tests

Hardness measurements were performed in arbitrarily selected areas of the rectangular samples using a Wilson Wolpert 402MVD hardness tester at constant load of 5 N and loading time of 15 s. At least ten hardness indentations were carried out in each condition to determine average as well as standard deviations.

To compare peak-hardness values after aging at 150°C and 190°C, tensile tests were performed using two samples for each condition to measure yield stress (YS), ultimate tensile strength (UTS) and elongation-to-fracture (*δ*). Flat 'dog-bone' samples, ~35 mm in length, ~7 mm in width and ~3 mm in thickness were used. The tensile curves were measured using an Instron 5882 tensile testing machine at an initial strain rate of ~10^{-3} s^{-1}.

2.3. TEM analysis

TEM specimens were cut, mechanically polished to the thickness of 100-200 μm and, finally electropolished with a solution of 2/3 methanol and 1/3 nitric acid at -30°C using a Struers TenuPol-5 twin-jet unit. Foils were studied in two microscopes operated at 200 kV: a JEOL JEM-2100F and a JEOL ARM-200F. The latter was equipped with a probe-aberration corrector and a JEOL ADF detector used in scanning mode. All the TEM settings are given in Table S1 (Supplementary Materials).

The ADF-STEM images taken in $<110>_{Al}$ and $<211>_{Al}$ zone axes (ZAs) were acquired to analyze the Ω plate bulk and interface structures. Crystal structures and elements occupying certain atomic columns were suggested from ADF-STEM images containing atomic number (Z) contrast [31]. For some images, fast Fourier transform (FFT) filtering was applied to reduce noise with a periodicity shorter than ~0.05 nm.

2.4.   Modelling and computations

Density functional theory (DFT) calculations were performed using Perdew-Burke-Ernzerhof (PBE) flavor [32] of the generalized gradient approximation (GGA) to exchange-correlation functional and standard PAW potentials [33] as implemented in the VASP program [34]. The key parameters are given in Table S2 (Supplementary Materials). Relaxation of the atom positions (p) but also full (f) relaxations (of atom position, cell geometry and volume) were carried out to refine the supercell configurations [26]. Note that p and f relaxations simulate two cases for the precipitate/matrix interactions considered as 'stiff' and 'weak' matrices, respectively. Thus, it may be presumed that the difference in formation energies after p and f relaxations for the supercells with the same plate thicknesses correlates with volumetric and structural incompatibilities between the precipitate and Al matrix lattices predicted in [7,28,29].

The formation energy was calculated as:

$$E_f = E_T - \sum_i \mu_i n_i \tag{5}$$

where E_T is the total energy of the slab consisting of N atoms, μ_i and n_i are the chemical potentials (see Table S3 in Supplementary Materials) and the number of i elements (Al, Cu, Mg and Ag) in the supercell, respectively.

All the calculations were done with the help of the SIMAN software package used for high-throughput DFT calculations [34]. Performed calculations can help to refine atom positions in the slab and to estimate the hypothetical interval for the precipitate formation energies. The Al lattice volume was chosen as a reference.

An orthorhombic supercell (SC) with different number of $\{111\}_{Al}$ layers applied in our DFT calculations was obtained from an ideal Al lattice ($a = 4.05$ Å, Fm-3m) using the transformation matrix P between the $[U\ V\ W]_{SC}$ and $[u\ v\ w]_{Al}$ basis vectors, expressed as:

$$\begin{bmatrix} U \\ V \\ W \end{bmatrix} = P \begin{bmatrix} u \\ v \\ w \end{bmatrix} \tag{1}$$

The transition matrix between an ideal Al lattice and orthogonal supercell can be described as follows:

$$P = \begin{bmatrix} -0.5 & -1.5 & k \\ 1 & 0 & k \\ -0.5 & 1.5 & k \end{bmatrix} \tag{2}$$

where $k \in R$ is proportional to supercell height normal to the broad plate interfaces.

Frozen phonon multi-slice simulations were carried out to obtain ADF-STEM images using the MULTEM software and the non-relativistic scattering potentials modified by Lobato et. al. [35–37]. ADF-STEM image simulations were carried out with Debye-Waller factors for Al, Cu, Mg, and Ag at 270 K from Peng et. al. [38]. In the simulations, sample thicknesses were chosen to be 100±10 nm for the $<110>_{Al}$ and $<211>_{Al}$ supercell projections. This sample thickness complies with 10 and 11 supercells in the respective lattice directions. MULTEM settings are given in Table S4 in Supplementary Materials.

3.   Results and Discussion

3.1.   High-resolution TEM observations

The samples peak-aged at 190°C for 1.5 h and at 150°C for 24 h were chosen for high-resolution TEM analysis [26,39]. Detailed analysis of the microstructure showed that the Ω plates aligned along $\{111\}_{Al}$ are a predominant strengthening agent in an Al-Cu-Mg-Ag alloy after peak-aging [26]. Note that the hardness evolutions for the samples during aging at 150°C and 190°C and the Ω plate morphologies in peak-aging stages are described in detail in Supplementary Materials (Figs. S1 and S2) and present in our previous works [26,39]. Our experimental observations support the fact that structural features discussed further regarding the Ω plates are not connected to peculiarities in their diameter distributions.
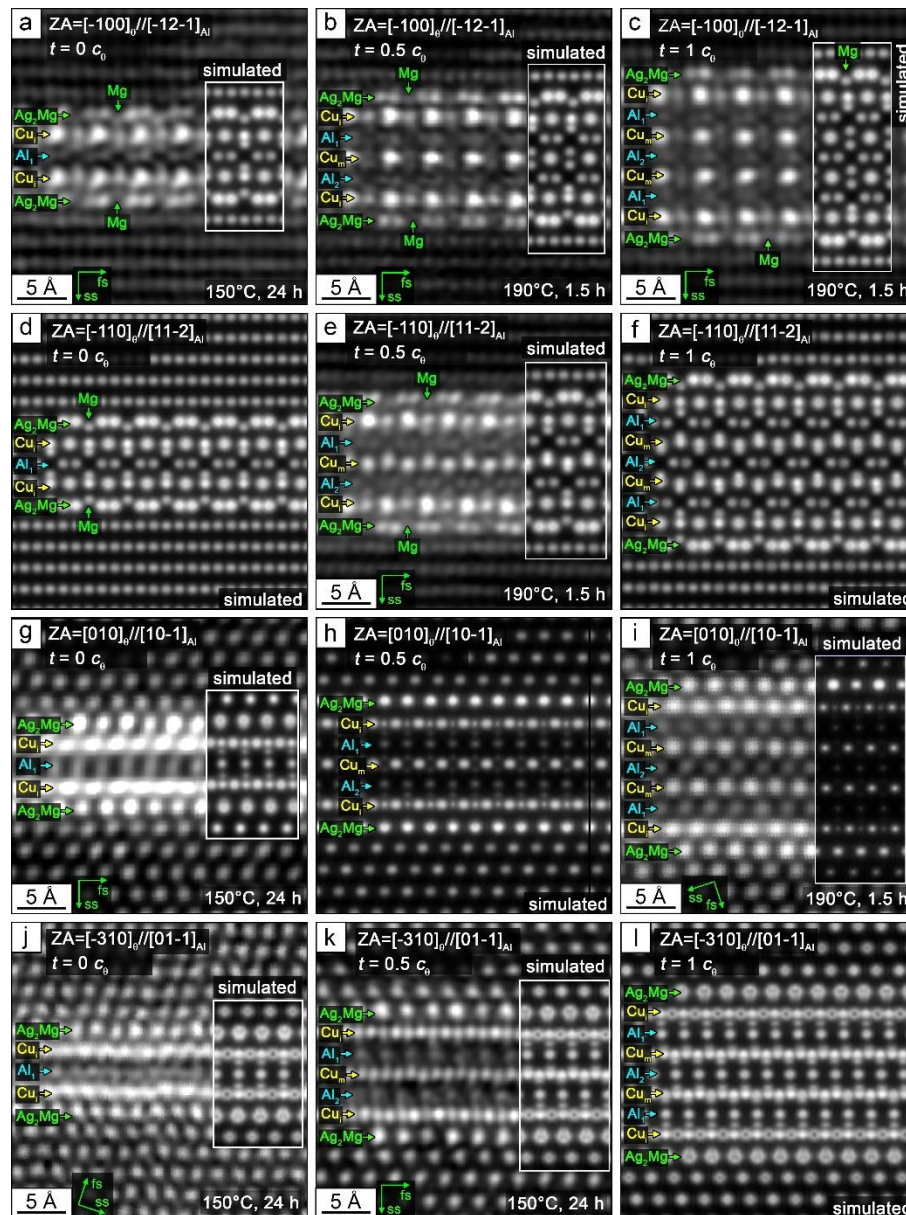
Figure 1. Experimental and simulated ADF-STEM images showing projections of the Ω plates with thicknesses (t) from 0 to 1 c_θ. The plates are shown in $[-100]_\theta$ (a-c), $[-110]_\theta$ (d-f), $[010]_\theta$ (g-i) and $[-310]_\theta$ ZAs (j-l). Experimental ADF-STEM images were FFT filtered. Fast and slow scanning directions are designated as 'fs' and 'ss', respectively. The simulated images were obtained using DFT supercells after p relaxations.

Experimental high-resolution ADF-STEM images taken along <110>$_{Al}$ and <112>$_{Al}$ ZAs and corresponded simulated ones are shown in Fig. 1. These images show cross-sections of the {111}$_{Al}$ plates in edge-on orientation. A careful analysis of the atomic column arrangements

enables us to conclude that these plates are constructed from interfacial boundaries and 'building blocks' with an orthorhombic structure closely linked to the equilibrium θ-phase (Al₂Cu, *I4/mcm*), which is typical for the Ω phase [4,7,11,15,17]. The 0.5 c_θ is related to the height of the ledges, whose nucleation and migration along broad interfaces cause the plate-like precipitate to thicken during aging at elevated temperatures [3,11,30,40].

The Ω plate thickness distribution has been analyzed using a set of ADF-STEM images. The results are summarized in Table 1 for both aging states. It has been found that a majority of the Ω plates has the thickness of 0.5 c_θ. It should also be noted in Table 1 that most of these plates have hybrid configuration, composing of orthorhombic θ and hexagonal η-phase fragments as described in [26]. The number fractions of hybrid precipitates are ~0.94 and 0.88 after aging at 150 °C and 190 °C, respectively (Table 1).

Table 1. Number of Ω plates with different thicknesses (relative to the orthorhombic θ unit cell in $[001]_\theta$ (c_θ)) identified from ADF-STEM images. Number of hybrid plates identified in each state are marked by asterisks.

Thickness, c_θ	0	0.5	1	1.5	2	2.5	3	3.5
24 h@150°C	12	33(31*)	-	1	2	0	1	-
1.5 h@190°C	15	40(35*)	3	5	4	-	-	-

The internal structure of the non-hybrid Ω plates, entirely comprising of the orthorhombic θ unit cells, can be represented as alternating Al_1 and Al_2 layers separated with Cu_m layers (see Fig. 1). In $(111)_{Al}/(001)_\theta$ projections Al_1 and Al_2 layers are displaced on a distance $a_\theta/2 \sim 2.5$ Å in $[-100]_\theta$ directions relative to each other. In Cu_i layers, Cu atoms occupy interstitial sites in comparison with Cu_m layers in the bulk orthorhombic θ structure [7,13].

Fig. 2 shows the edge interface structure for the Ω plates and corresponding thicknesses imaged by ADF-STEM. It is clearly seen that there is no misfit compensating dislocation at the edge interface of the plates with thickness less or equal 2 c_θ. A single misfit-compensating dislocation appears in the plates thicker than or equal to 3 c_θ (Fig. 2). Thus, our experimental observations are consistent with [3,11], where the misfit-compensating dislocation spacing was found to be 2.5-3 c_θ for the thick plates in an Al-Cu-Mg-Ag alloy over-aged at 200-375°C. Note that, as a result, we can directly link atomic layers inside the Ω phase (Cu_m, Al_1 and Al_2) as well

as at Al/Ω interfaces (Ag_2Mg and Cu_i) to the Al matrix stacking (*A*, *B* and *C*) in our modelling for the plates with thicknesses up to ~2…2.5 $c_θ$.
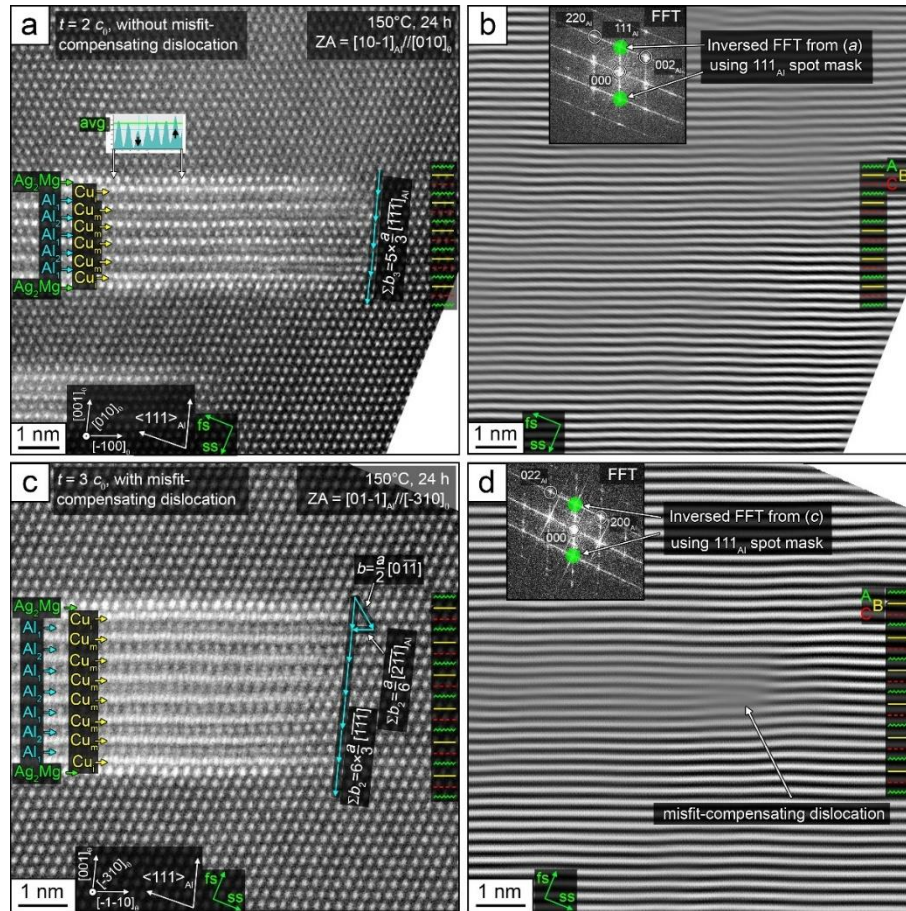

Figure 2. The {111}$_{Al}$ plates without (a, b) and with (c, d) a misfit-compensating dislocation (MCD) and corresponding thicknesses (*t* in $c_θ$) imaged by ADF-STEM. The FFT images were inversed by the 111$_{Al}$ spot masked (b, d) to show the appearance of a misfit-compensating dislocation as a Frank partial dislocation with $\vec{b}=a/3[111]_{Al}$ [3,11]. For each image, the fast and the slow scanning directions are designated as 'fs' and 'ss', respectively. The [-1-1-1]$_{Al}$ direction is shown to clarify the presence of image drifting. To show compatibility between the plate internal structure and the Al matrix, *A*, *B* and *C* stacking layers have been marked by yellow solid, red dashed and green saw-tooth lines, respectively. Note that in the given projections the edge interfaces of Ω plates are overlayed with the adjacent Al matrix along the viewing direction in ADF-STEM images.

Another feature found in ADF-STEM images is that image intensity distribution is non-uniform along the Ag_2Mg interface layer for the plates with different thicknesses (example of the

intensity profile in Fig. 2a). This can indicate a possible deviation from the interface stoichiometric composition or vacancy presence in the interface structure compared to the energetically favorable configuration described by Kang et al [7] and used in our calculations. Kang et al. [7] also predicted that certain atomic columns in the Ag$_2$Mg layers can be enriched by other elements like Al or Cu, due to strain accommodation and interface energy minimization mechanisms activated by incompatibility between precipitate and matrix lattices.

3.2.   Modelling and computations

First-principles calculations have been performed in the present work to find energetically favorable atomic configurations for the supercells containing non-hybrid Ω plates, entirely comprising of the orthorhombic θ lattice [7,17], embedded in the Al matrix, as well as to assess volumetric and structural compatibility between the precipitate and the matrix lattices. For this, supercell parameters such as sizes and angles in addition to total energies and formation enthalpies after f relaxations were compared with that after p relaxations for the Ω plates with different thicknesses.

3.2.1   Construction of the supercells

In the present study, DFT supercells were constructed with non-hybrid $\{111\}_{Al}$ Ω plates involving bulk and interface structures. The bulk structure was based on orthorhombic θ unit cells with $a_\theta = 4.96$ Å, $b_\theta = 8.56$ Å and $c_\theta = 8.48$ Å [4]. The periodic bulk θ unit cell structure can be represented as: …-Cu$_m$-Al$_1$-Cu$_m$-Al$_2$-… layers displacing $\{111\}_{Al}$ planes [4,7,26] as shown in Figs. 1 and 2a, c.

The broad Ω plate interfaces include energetically favorable Ag$_2$Mg and Cu$_i$ layers [7,13] that connect the precipitate to matrix $\{111\}_{Al}$ planes creating the following order of layers: Al(matrix)-Ag$_2$Mg-Cu$_i$-Al$_1$(or Al$_2$) (precipitate). The incorporation of these sandwich-like precipitate structures into the Al matrix having A, B and C stackings along $<111>_{Al}$ imposes volumetric and structural restrictions. As a result, significant shear components [28,29] as well as misfit strains [11,15,21,27] can appear along the broad plate interfaces due to structural and volumetric incompatibility, respectively, between the precipitate and matrix lattices [26].

It should be noted that the Ω plate thicknesses (t) modelled in supercells varied from 0 to 2.5 c_θ with the step of 0.5 c_θ in $[001]_\theta//[111]_{Al}$ [7,26]. The supercells with 0 c_θ thick Ω plates contain Ag$_2$Mg and Cu$_i$ interface layers as well as a single, hexagonal Al atom layer (Figs. 1a, d, g and j). For this reason, this thickness cannot be referenced to 0.5 c_θ thick plates.

3.2.2 Effect of the inter-precipitate spacings on supercell energy and its geometry

Since we applied supercells with periodic boundary conditions, their convergence over the inter-precipitate spacing (N) have been evaluated. N, i.e. a number of $\{111\}_{Al}$ planes, varied in range from 5 to 20 with the step of 3 to avoid the formation of a stacking fault in $[111]_{Al}$.

Supercells tend to relieve precipitate/matrix incompatibility by their lattice distortion (compared to precipitate/matrix equilibrium lattices) after p relaxations, while supercell geometries can be optimized with a low level of elastic strains relieved after f relaxations. We obtained in our previous work that elastic strains after f relaxations can be relieved by supercell transformation in two shear directions called here as shear components: $[-101]_{Al}//[0-10]_\theta$ (τ_I) and $[1-21]_{Al}//[100]_\theta$ (τ_{II}). Note that supercells with 0.5 c_θ thick plates have been found to be energetically favorable with τ_I instead of less stable τ_{II} [26]. The presence of these shear components in $\{111\}_{Al}$ in different supercell configurations after p relaxations can be represented as cooperative atom shifts in the respective plane in comparison with the ideal orthorhombic θ and Al lattices after p relaxations. Note that these shifts occur on distances shorter than the precipitate and matrix lattice parameters. As a result of f relaxations, the initially orthorhombic supercell shape may transform to a monoclinic one with similar cooperative atomic shifts.
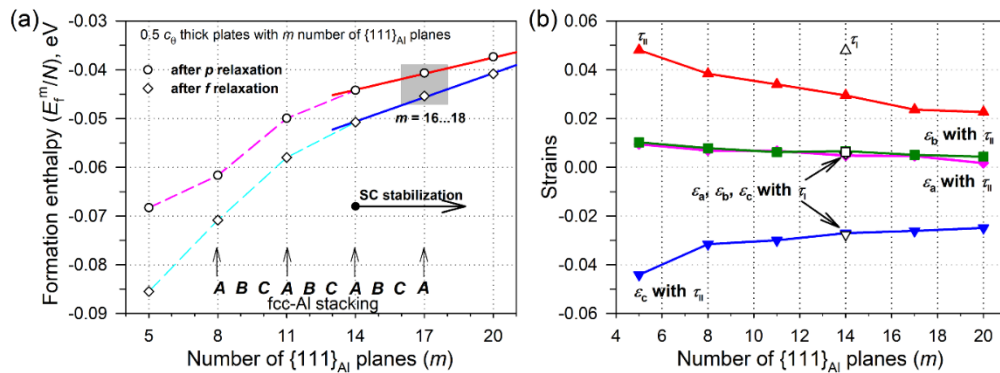

Figure 3. Effect of the number of $\{111\}_{Al}$ planes (m) in supercells (SCs) containing 0.5 c_θ thick plates on formation enthalpies normalized to the total atom numbers (N) (a) and strains in SC obtained after f relaxations. Shear components (τ) were estimated as $|\tau| = |tg(\pi-\lambda)|$, where λ is the spatial angle combing basic for the DFT supercells after f relaxations. To estimate linear strains (ε_a, ε_b and ε_c) the Al lattice volume was chosen as a reference. Stabilization of SC is seen at more than ~14 $\{111\}_{Al}$ planes.

Changes in the formation enthalpies per atom in supercells with different numbers of $\{111\}_{Al}$ planes (m) and supercell parameters (sizes and angles) after f relaxations are shown in Fig. 3a and b, respectively. Shear components reflecting precipitate/matrix structural incompatibility were estimated as $\tau = |tg(\pi-\lambda)|$, where λ is the spatial angle combing basic vector orientations in DFT supercells after f relaxations. The precipitate/matrix volumetric incompatibility was defined as a misfit strain: $\varepsilon_{[uvw]Al} = (x_f - x_p)/x_p$, where x_p and x_f are DFT supercell sizes ($a//[-12-1]_{Al}$, $b//[-101]_{Al}$, and $c//[111]_{Al}$ after p and f relaxations, respectively. Example of influence of shear components τ_I and τ_{II} discussed in previous paragraph on supercell geometry is also given in Fig. 3b.

Obvious effect of the number of $\{111\}_{Al}$ planes on formation enthalpies as well as supercell parameters have been found (Fig. 3). Coherent strain fields at a low number of the planes, i.e., small inter-precipitate spacings, are seen to interfere from neighbor precipitates. Stabilization of supercell configurations is seen to occur when the number of planes is more than 14.

Therefore, such DFT supercells were constructed (1) to find energetically favorable shear component directions for the plates with different thicknesses and (2) to parameterize precipitate/matrix volumetric and structural incompatibilities.
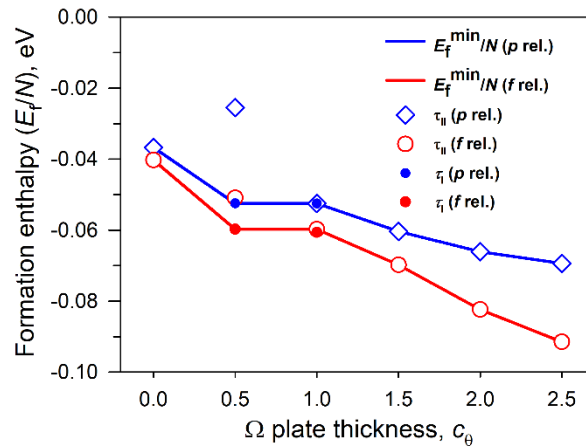

Figure 4. Effect of the plate thicknesses and $[-101]_{Al} // [0-10]_\theta$ or $[1-21]_{Al} // [100]_\theta$ shear components on the formation enthalpies calculated by DFT after p relaxations. The supercell (SCs) with 21 $\{111\}_{Al}$ planes ($k=7$) was chosen as a reference. Supercell with 0.5 and 1 c_θ thick plates are seen to be energetically favorable with shear component τ_I and τ_I/τ_{II}, respectively. During relaxations supercells involving 0, 1.5, 2.5 c_θ thick plates with τ_I transformed to the one with τ_{II}. Note that comparing all supercells 2 c_θ thick plates have shear component τ_{II} close to zero.

3.2.3 Energetically favorable shear component directions

Some supercells were constructed with the same height of 21 {111}$_{Al}$ planes, with part of them being substituted by the Ω plates with different thicknesses. As a result, the number of {111}$_{Al}$ planes decreased from 16 to 5 for the supercells involving 0 and 2.5 c_θ thick plates. Note that all these supercells had the same total number of different sorts of atoms (Al, Cu, Mg and Ag).

The effect of [-101]$_{Al}$ // [0-10]$_\theta$ and [1-21]$_{Al}$ // [100]$_\theta$ shear components have been analyzed on supercells after p and f relaxations (Fig. 4). Combining formation enthalpies, generalized in Fig. 4, with typical supercell configurations refined after p relaxations, shown in Fig. 5, help us to find relationships between energetically favorable shear components and the plate thicknesses:

i. The first type of supercells with the plate thicknesses of 0, 1.5 and 2.5 c_θ demonstrates only one energetically favorable [1-21]$_{Al}$ // [100]$_\theta$ shear component (τ_{II}).

ii. The second type involves only 0.5 c_θ thick plates with energetically favorable [-101]$_{Al}$ // [0-10]$_\theta$ shear component (τ_I) [26]. Supercells involving 0.5 c_θ thick plates with τ_{II} are less stable due to a significant absolute value required to provide a supercell convolution as seen in Fig. 3b. Note that the difference in formations enthalpies of the supercells with τ_I and τ_{II} is significantly smaller for 1-1.5 c_θ thick plates in comparison with supercells involving 0.5 c_θ thick plates.

iii. The third type of supercells involving 1 c_θ thick plates can have energetically favorable configuration with both shear components τ_I and τ_{II}. Using equations given in Section 3.2.2., shear components (τ) / misfit strains in [111]$_{Al}$/[001]$_\theta$ (ε_c) were estimated to be 0.037/-0.001 and 0.031/-0.032 in the cases with shear components τ_I and τ_{II}, respectively. Thus, atomic configurations in the supercells keep a balance between energies of misfit strains in [111]$_{Al}$//[001]$_\theta$ and the respective shear strains [26]. Increase in the interplane spacing ($d_{[111]Al}$) are known to promote reducing shear strain field energy (E_S) being inversely proportional to $d_{[111]Al}$ ($E_S \sim 1 / d_{[111]Al}$) [41].

iv. Unlike the first, second and third types of supercells containing plates with different τ orientations, the fourth one with 2 c_θ thick plates have shear component close to zero. These plates are well matching the Al matrix if there are no misfit-compensating dislocations at the edge interfaces (Figs. 2c and d). Note that 2 c_θ thick plates have volumetric incompatibility related to a significant unrelaxed misfit in [111]$_{Al}$ // [001]$_\theta$ [15,21,27]. This misfit strain is known to increase with increasing the plate thickness

[15,21,27]. In addition, the difference in formation enthalpies for the supercells after p and f relaxations can be directly linked to a 'pure' elastic strain energy accumulated in the structure due to volumetric precipitate/matrix incompatibility in $[111]_{Al}//[001]_\theta$.

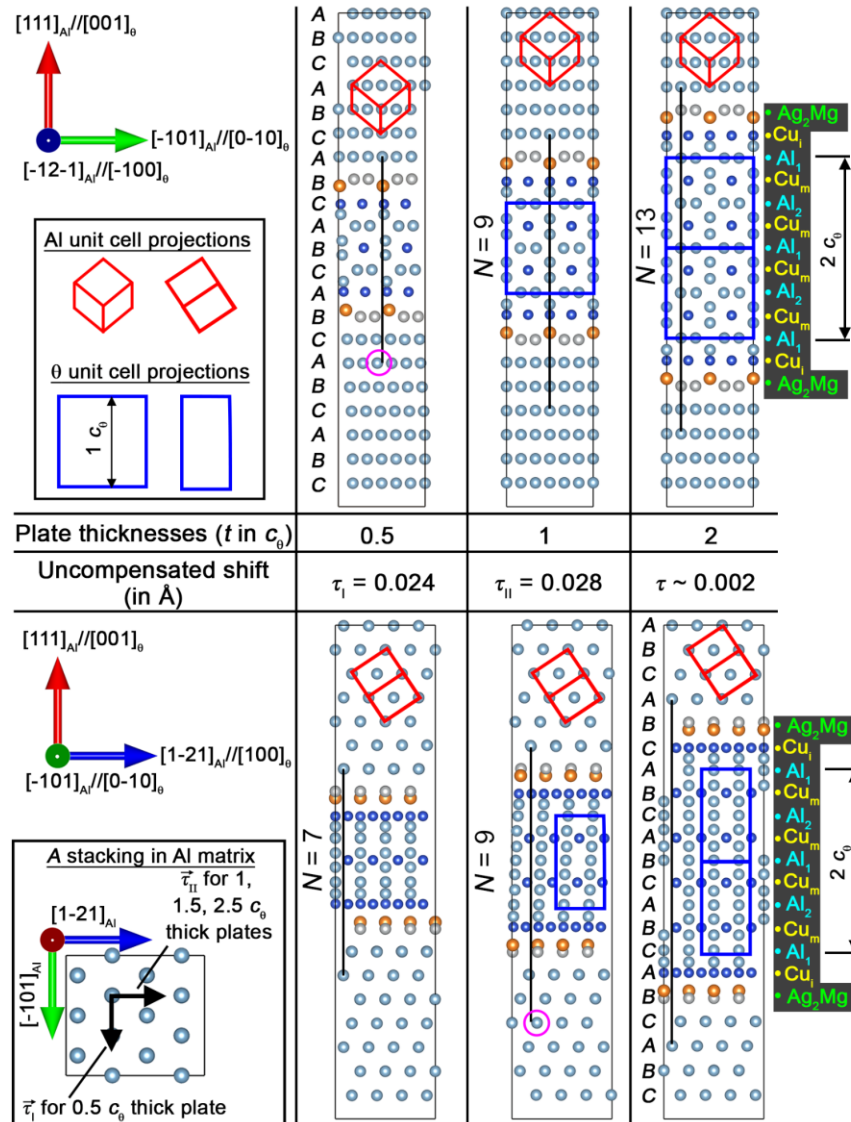Figure 5. Typical $[-12-1]_{Al}$ and $[-101]_{Al}$ projections of supercells containing Ω plates with thicknesses of 0.5, 1 and 2 c_θ after p relaxation. Examples of cooperative atom shifts related to $[-101]_{Al} // [0-10]_\theta$ (τ_I) and $[1-21]_{Al} // [100]_\theta$ (τ_{II}) shear components are marked by black solid line and purple circle for 0.5 and 1 c_θ thick plates. There is no uncompensated shift in the supercells with 2 c_θ thick plates. N is the number of $\{111\}_{Al}$ planes substituted by the precipitates.

To verify our precipitate structures refined by DFT, the most energetically favorable supercells after p relaxations were used to simulate ADF-STEM images shown in Fig. 1. It is seen that experimental and simulated ADF-STEM images are similar to each other by atomic column positions in several precipitate projections. Insignificant differences in atomic column intensity distributions can be caused by the same Debye-Waller factors used for all elements as well as a defocus plane position in the MULTEM software. Note that Kang et al. [7] suggested that interfacial substitutions in Ag_2Mg and Cu_i layers operate as strain accommodation and free energy minimization mechanisms, which can cause the observed discrepancies in simulated and experimental ADF-STEM images. In addition, Yang et al. [16] also showed that Al_2Mg interfacial layers can be a slightly more energetically favorable than Ag_2Mg, indicating a possible full or even partial substitution of Ag by Al atoms.

Table 2. DFT results of formation energies for the supercells involving plates with thicknesses up to 2.5 c_θ. Formation energies of the structures were calculated after atom position (p) and full (f) relaxations (R). N_L and N_{Al} are the number of $\{111\}_{Al}$ layers and Al atoms substituted by the precipitate slab in each supercell, respectively. Supercell parameters a, b and c are along [-12-1]$_{Al}$ // [-100]$_\theta$, [-101]$_{Al}$//[010]$_\theta$ and [111]$_{Al}$ // [001]$_\theta$, respectively.

Plate thickness, c_θ	N_L (N_{Al})	R	E_T, eV	E_f, eV	Supercell parameters		Shear components
					Sizes, Å	Angles, °	
0	5 (60)	p	-936.1	-9.4	9.9×8.6×49.1	90×90×90	-
		f	-937.0	-10.3	10.0×8.6×48.1	90×92×90	$\tau_{II} = 0.035$
0.5	7 (84)	p	-1074.2	-11.9	9.9×8.6×56.1	90×90×90	-
		f	-1075.6	-13.2	10×8.6×54.6	88.7×90.1×90	**$\tau_I = 0.024$**
1	9 (108)	p	-1212.1	-14.2	9.9×8.6×63.1	90×90×90	-
		f	-1213.6	-15.6	9.9×8.6×61.6	90×88.4×90	$\tau_{II} = 0.028$
1.5	11 (132)	p	-1215.1	-16.3	9.9×8.6×63.1	90×90×90	-
		f	-1272.2	-18.4	9.9×8.6×61.0	90×89.4×90	$\tau_{II} = 0.010$
2.0	13 (156)	p	-1353.0	-18.5	9.9×9.9×70.1	90×90×90	-
		f	-1355.9	-21.4	9.9×8.6×67.7	90×89.9×90	$\tau_{II}\sim0.002$
2.5	15 (180)	p	-1490.7	-20.6	9.9×8.6×77.1	90×90×90	-
		f	-1494.2	-24.2	9.9×8.6×74.3	90×90.9×90	$\tau_{II} = 0.016$

3.2.4 Precipitate/matrix volumetric and structural incompatibility parametrization

Supercells with N in the range from 16 to 18 $\{111\}_{Al}$ planes (Fig. 3a) were constructed to put the precipitates with thicknesses from 0 to 2.5 c_θ in the same structural condition to reduce the

effect of inter-precipitate spacings. In this case, the total atom number varied from 256 to 400 for the supercells involving 0 and 2.5 c_θ thick plates, respectively. Note that different, but close inter-precipitate spacing (16-18 $\{111\}_{Al}$) were used for the supercell convolution without a stacking fault along $[111]_{Al}$.

Energetically favorable shear components τ_I and τ_{II} were applied in supercells with 0.5 c_θ thick plates and 0, 1, 1.5 and 2.5 c_θ thick plates, respectively. Supercell geometry parameters like sizes and angles, as well as formation enthalpies are summarized in Fig. 6 and Table 2.
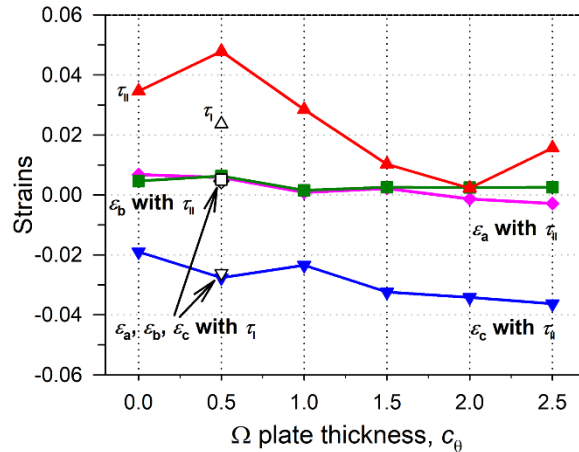

Figure 6. Precipitate/matrix incompatibility parameterized in misfit strains (ε) and shear components τ_I ($[-101]_{Al}$ // $[0-10]_\theta$) and τ_{II} ($1-21]_{Al}$ // $[100]_\theta$) in supercells after f relaxations.

Analysis of relationships between the plate thickness and τ/ε values shows that misfit strains $\varepsilon_{[-12-1]Al}$ and $\varepsilon_{[-101]Al}$ slightly change in the ranges of +0.7…-0.3% and +0.5…+0.3%, respectively, due to structural incompatibility in $(111)_{Al}//(001)_\theta$ planes. Thus, these parameters are seen not to provide significant supercell deformations in comparison with $\varepsilon_{[111]Al}$. $\varepsilon_{[111]Al}$ linearly increases from 2.6 to 3.6% as the plate thicknesses increase from 0.5 to 2.5 c_θ, or may be from 2.4 to 3.6% for 1 and 2.5 c_θ thick plates. It yields misfit increment in the range from 0.25 to 0.40% per half orthorhombic θ unit cell (a conventional thickening ledge height for the Ω plates [3,7,11]). Note that $\varepsilon_{[111]Al}$ for the bulk orthorhombic θ structure was previously evaluated to be 9.3% on the basis of lattice parameters alone [11,15,21,27], or it changed in the order of 0, +5, 0,-5, 0% as experimentally measured for the Ω plates with the thicknesses of 0, 0.5, 1, 1.5, and 2 c_θ, respectively, by Kang et al. [7]. Note that discrepancy between our results and the latter estimated by Kang et al. may be caused by the experimental method used to measure this parameter.

It is interesting to note that 0 c_θ thick plates including Ag_2Mg, Cu_i and Al_1 (or Al_2) layers may have a relatively large misfit strain of -1.9 % (Fig. 6). A half of this stack height (-0.95%) should be connected to $\{111\}_{Al}$ stacking of the matrix if a single thickening ledge forms. Taking into account the ideal interface structures suggested by Kang et al. [7] as well as the case with 'weak' Al matrix in our modelling, we can conclude that misfit strains distribute non-uniformly across the plate thickness ($[111]_{Al} // [001]_\theta$). Large misfit strains concentrate at the broad interfaces, i.e. in Ag_2Cu and Cu_i layers. Hutchinson et al. [11] considered a strong vacancy (tension) misfit strain to be a very unfavorable condition for the nucleation of a single coherent, thickening ledge on the broad Ω surfaces. Thus, we also can connect this predominant misfit strain concentration at the broad interfaces to a high thermal resistance to thickening for the Ω plates, because it increases the nucleation barrier for a coherent ledge. This takes place despite the fact that the presence of Mg and Ag at the θ/Al interface can dramatically facilitate the Ω precipitate formation [15,16].

3.2.5 Precipitation sequence

Our DFT calculations show that a re-orientation of shear components is required to keep energetically favorable precipitate configurations in the Al matrix, by reducing energy of the strain fields surrounding them during the plate thickening process. Using DFT results as well as our experimental observations, the precipitation sequence during aging can be written as

0 c_θ plates (τ_{II}) - hybrid 0.5 c_θ plates ($\tau{\sim}0$) - 0.5 c_θ plates (τ_I) - 1 c_θ plates (τ_I or τ_{II})- 1 c_θ plates (τ_{II})

The formation of hybrid precipitates can be a result of their unstable chemistry at the early aging stages. As shown in Fig. 4, 0.5 c_θ thick plates with shear component τ_I is more energetically favorable in comparison with the same supercells with shear components τ_{II}. Comparing the energy differences of 0.5 c_θ thick plates with τ_I and τ_{II} and 1-1.5 c_θ thick plates with the same shear components, formation of the former ones with τ_{II} seems to be energetically prohibited in the Al-Cu-Mg-Ag alloy.

The same formation enthalpies of supercells involving 1 c_θ thick plates with shear components τ_I and τ_{II} in comparison with 0.5 c_θ thick ones after p and f relaxations (Fig. 4) make us conclude that 1 c_θ thick plates with τ_I may form earlier than that with τ_{II} during aging. Moreover, considering further precipitate thickening processes, the shear component τ_{II} is more energetically favorable in the supercells involving the Ω plates with thicknesses of 1.5 c_θ.

Since hybrid precipitate configurations have not been found among the relatively thick Ω plates in the studied alloy after peak-aging it suggests that non-hybrid plates are slightly more stable than hybrid ones. Analysis of the precipitate structures in Al-Cu-Mg-Ag alloys did not show the presence of hybrid Ω plates after aging at higher temperatures as well [3,11]. However, hybrid Ω precipitates are seen in the present work to be responsible for the main contribution to the strength of the alloy after peak aging [8,26]. It occurs despite the fact that this precipitate does not have shear components as well as related shear strain fields surrounding the plates, but a bit larger misfit strains in $[111]_{Al}$ // $[001]_\theta$ in comparison with non-hybrid ones [26]. Note that if plastic deformation in Al-Cu-Mg-Ag alloys is attributed to shearing of disperse Ω plates [10,42–44], any heterogeneity in precipitate structures may require additional stress to cut them. As a result, the strength of the alloys with hybrid plates should be higher than that in the alloys involving non-hybrid ones [45].

Conclusion

The morphology and structure of the Ω plates with different thicknesses have been analyzed in an Al-Cu-Mg-Ag alloy peak-aged at 150°C for 24 h and 190°C for 1.5 h by high-resolution ADF-STEM and DFT calculations. The results can be summarized as follows:

1. The precipitate/matrix structural incompability was found to change depending on the Ω plate thicknesses during aging. Two types of shear components: $[-101]_{Al}$ // $[0-10]_\theta$ (τ_I) and $[1-21]_{Al}$ // $[100]_\theta$ (τ_{II}) were predicted by DFT calculations. Shear component τ_I has been found to be energetically favorable only with 0.5 c_θ thick plates. Comparing τ_I and τ_{II} absolute values in supercells involving the plates with different thicknesses, plates with thickness 2 c_θ have the shear component τ close to zero.

2. Volumetric incompatibility between non-hybrid Ω precipitates comprising orthorhombic θ unit cells and the Al matrix was estimated for the plates with thickness from 0 to 2.5 c_θ. Volumetric incompatibility causes the formation of misfit strain normal to the broad plate interfaces along $[111]_{Al}$. This misfit strain distributes non-uniformly across the plate thickness. Misfit strain between Ag_2Cu/Cu_i layers and the Al matrix is about 2-4 times larger than that between a half of orthorhombic θ unit cell height (0.5 c_θ) and the respective matrix. This phenomenon can be directly related with a prohibitively high barrier to ledge nucleation resulting in a high thermal resistance to thickening of the Ω precipitates.

3. The precipitation sequence during aging can be written as

0 c_θ plates (τ_{II}) - hybrid 0.5 c_θ plates ($\tau \sim 0$) - 0.5 c_θ plates (τ_I) - 1 c_θ plates (τ_I or τ_{II}) - 1 c_θ plates (τ_{II}).

Hybrid 0.5 c_θ thick plates with $\tau \sim 0$ provide the main contribution to the strength of Al-Cu-Mg-Ag alloy.

Acknowledgment

Declaration of competing interest

The authors declare that they have no known competing financial interests or personal relationships that could have appeared to influence the work reported in this paper.

Data availability

The raw/processed data required to reproduce these findings cannot be shared at this time as the data also forms part of an ongoing study.

References

[1]   I.J. Polmear, Light alloys: from traditional alloys to nanocrystals, third ed., Butterworth-Heinemann/Elsevier, Oxford (UK), 2006.

[2]   J.F. Nie, Physical Metallurgy of Light Alloys, Fifth Edit, Elsevier, 2014. https://doi.org/10.1016/B978-0-444-53770-6.00020-4.

[3]   R.W. Fonda, W.A. Cassada, G.J.J. Shiflet, Accommodation of the misfit strain surrounding {III} precipitates (Ω) in Al-Cu-Mg-(Ag), Acta Metall. Mater. 40 (1992) 2539–2546.

[4]   K.M. Knowles, W.M. Stobbs, The structure of {111} age-hardening precipitates in Al-Cu-Mg-Ag alloys, Acta Crystallogr. Sect. B Struct. Sci. 44 (1988) 207–227. https://doi.org/10.1107/S0108768187012308.

[5]   J.H. Auld, Structure of metastable precipitate in some Al–Cu–Mg–Ag alloys, Mater. Sci. Technol. 2 (1986) 784–787. https://doi.org/10.1179/mst.1986.2.8.784.

[6]   S. Kerry, V.D. Scott, Structure and orientation relationship of precipitates formed in Al-Cu-Mg-Ag alloys, Met. Sci. 18 (1984) 289–294. https://doi.org/10.1179/030634584790420069.

[7]   S.J. Kang, Y.W. Kim, M. Kim, J.M. Zuo, Determination of interfacial atomic structure, misfits and energetics of Ω phase in Al-Cu-Mg-Ag alloy, Acta Mater. 81 (2014) 501–511. https://doi.org/10.1016/j.actamat.2014.07.074.

[8]   M. Gazizov, R. Kaibyshev, Precipitation structure and strengthening mechanisms in an Al-Cu-Mg-Ag alloy, Mater. Sci. Eng. A. 702 (2017) 29–40. https://doi.org/10.1016/j.msea.2017.06.110.

[9]   M. Gazizov, R. Kaibyshev, Effect of pre-straining on the aging behavior and mechanical properties of an Al-Cu-Mg-Ag alloy, Mater. Sci. Eng. A. 625 (2015) 119–130. https://doi.org/10.1016/j.msea.2014.11.094.

[10]   M. Gazizov, R. Kaibyshev, High cyclic fatigue performance of Al-Cu-Mg-Ag alloy under T6 and T840 conditions, Trans. Nonferrous Met. Soc. China (English Ed. 27 (2017). https://doi.org/10.1016/S1003-6326(17)60142-0.

[11]   C.R. Hutchinson, X. Fan, S.. Pennycook, G.. Shiflet, On the origin of the high coarsening resistance of Ω plates in Al–Cu–Mg–Ag Alloys, Acta Mater. 49 (2001) 2827–2841. https://doi.org/10.1016/S1359-6454(01)00155-0.

[12]   L. Sun, D.L. Irving, M. a. Zikry, D.W. Brenner, First-principles investigation of the structure and synergistic chemical bonding of Ag and Mg at the Al|Ω interface in a Al–Cu–Mg–Ag alloy, Acta Mater. 57 (2009) 3522–3528. https://doi.org/10.1016/j.actamat.2009.04.006.

[13]   S.J. Kang, J.-M. Zuo, H.N. Han, M. Kim, Ab initio study of growth mechanism of omega precipitates in Al-Cu-Mg-Ag alloy and similar systems, J. Alloys Compd. 737 (2018) 207–212. https://doi.org/10.1016/J.JALLCOM.2017.12.010.

[14]   S. Abis, P. Mengucci, G. Riontino, A study of the high-temperature ageing of Al-Cu-Mg-Ag alloy 201, Philos. Mag. B Phys. Condens. Matter; Stat. Mech. Electron. Opt. Magn. Prop. 67 (1993) 465–484. https://doi.org/10.1080/13642819308207686.

[15]   B.C. Muddle, I.J. Polmear, The precipitation Ω phase in Al-Cu-Mg-Ag alloys, Acta Metall. 37 (1989) 777–789. https://doi.org/10.1016/0001-6160(89)90005-9.

[16]   S.L. Yang, N. Wilson, J.F. Nie, Revisit of the structure of Ω precipitate in Al-Cu-Mg-Ag alloys, Scr. Mater. 205 (2021) 114204. https://doi.org/10.1016/j.scriptamat.2021.114204.

[17]   S.C. Wang, M.J. Starink, Precipitates and intermetallic phases in precipitation hardening Al–Cu–Mg–(Li) based alloys, Int. Mater. Rev. 50 (2005) 193–215. https://doi.org/10.1179/174328005X14357.

[18]   D. Vaughan, J.M. Silcock, The orientation and shape of θ precipitates formed in an Al-Cu alloy, Phys. Status Solidi. 20 (1967) 725–736. https://doi.org/10.1002/pssb.19670200235.

[19]   A. Garg, Y.C. Chang, J.M. Howe, Precipitation of the Ω phase in an Al-4.0Cu-0.5Mg alloy, Scr. Metall. Mater. 24 (1990) 677–680. https://doi.org/10.1016/0956-

716X(90)90222-3.

[20]   K. Hono, T. Sakurai, I.J. Polmear, Pre-precipitate clustering in an Al-Cu-Mg-Ag alloy, Scr. Metall. Mater. 30 (1994) 695–700. https://doi.org/10.1016/0956-716X(94)90184-8.

[21]   S.P. Ringer, K. Hono, I.J. Polmear, T. Sakurai, Nucleations of precipitates in aged Al-Cu-Mg-(Ag) alloys with high Cu:Mg ratios, Acta Mater. 44 (1996) 1883–1898.

[22]   K. Hono, N. Sano, S.S. Babu, R. Okano, T. Sakurai, Atom probe study of the precipitation process in AlCuMgAg alloys, Acta Metall. Mater. 41 (1993) 829–838. https://doi.org/10.1016/0956-7151(93)90016-L.

[23]   L. Reich, M. Murayama, K. Hono, Evoultion of Ω phase in an Al-Cu-Mg-Ag alloy - A three dimensional atom probe study, Acta Mater. 46 (1998) 6053–6062.

[24]   Y.C. Chang, J.M. Howe, Composition and stability of Ω- phase in an Al-Cu-Mg-Ag alloy, Metall. Trans. A. 24A (1993) 1461–1470.

[25]   J.M. Howe, Analytical transmission electron microscopy analysis of Ag and Mg segregation to { 111 } θ precipitate plates in an Al-Cu-Mg-Ag alloy, Philos. Mag. Lett. 70 (1994) 111–120. https://doi.org/10.1080/09500839408240963.

[26]   M.R. Gazizov, A.O. Boev, C.D. Marioara, S.J. Andersen, R. Holmestad, R.O. Kaibyshev, D.A. Aksyonov, V.S. Krasnikov, The unique hybrid precipitate in a peak-aged Al-Cu-Mg-Ag alloy, Scr. Mater. 194 (2021) 113669. https://doi.org/10.1016/j.scriptamat.2020.113669.

[27]   A. Garg, J.M. Howe, Convergent-beam electron diffraction analysis of the Ω phase in an Al-4.0Cu-0.5Mg-0.5Ag alloy, Acta Metall. Mater. 39 (1991) 1939–1946.

[28]   H.I. Aaronson, B.C. Muddle, J.F. Nie, On recent developments in the debate about the formation mechanism of precipitate plates, Scr. Mater. 41 (1999) 203–208. https://doi.org/10.1016/S1359-6462(99)00144-X.

[29]   J.F. Nie, H.. Aaronson, B.C. Muddle, The formation of precipitate plates and their role in the strengthening of aluminium alloys, in: M. Tiyakioglu, M. Tiyakioglu (Eds.), Adv. Metall. Alum. Alloy., Indianapolis, 2001: pp. 229–238.

[30]   D.A. Porter, K.E. Easterling, M.Y. Sherif, Phase transformations in metals and alloys, third ed., CRC press, New York, 2014.

[31]   P.D. Nellist, S.J. Pennycook, The principles and interpretation of annular dark-field Z-contrast imaging, in: 2000: pp. 147–203. https://doi.org/10.1016/S1076-5670(00)80013-0.

[32]   J.P. Perdew, K. Burke, M. Ernzerhof, Generalized gradient approximation made simple, Phys. Rev. Lett. 77 (1996) 3865.

[33]   E. Blochl, Projector Augmented-Wave Method, Phys. Rev. B. 50 (1994) 17953–17979. https://doi.org/10.1103/PhysRevB.50.17953.

[34]   G. Kresse, J. Furthmüller, Efficient iterative schemes for ab initio total-energy calculations using a plane-wave basis set, Phys. Rev. B - Condens. Matter Mater. Phys. 54 (1996) 11169–11186. https://doi.org/10.1103/PhysRevB.54.11169.

[35]   I. Lobato, S. van Aert, J. Verbeeck, Progress and new advances in simulating electron microscopy datasets using MULTEM, Ultramicroscopy. 168 (2016) 17–27. https://doi.org/10.1016/j.ultramic.2016.06.003.

[36]   I. Lobato, D. Van Dyck, MULTEM: A new multislice program to perform accurate and fast electron diffraction and imaging simulations using Graphics Processing Units with CUDA, Ultramicroscopy. 156 (2015) 9–17. https://doi.org/10.1016/j.ultramic.2015.04.016.

[37]   I. Lobato, D. Van Dyck, An accurate parameterization for scattering factors, electron densities and electrostatic potentials for neutral atoms that obey all physical constraints, Acta Crystallogr. Sect. A Found. Adv. 70 (2014) 636–649. https://doi.org/10.1107/S205327331401643X.

[38]   L.M. Peng, G. Ren, S.L. Dudarev, M.J. Whelan, Debye-Waller factors and absorptive scattering factors of elemental crystals, Acta Crystallogr. Sect. A Found. Crystallogr. 52 (1996) 456–470. https://doi.org/10.1107/S010876739600089X.

[39]   M. Gazizov, R. Holmestad, R. Kaibyshev, Comparative analysis of the microstructure and mechanical properties of an Al-Cu-Mg-Ag alloy peak-aged at relatively low and high temperatures, in: IOP Conf. Ser. Mater. Sci. Eng., 2019. https://doi.org/10.1088/1757-899X/672/1/012027.

[40]   M. Gazizov, R. Kaibyshev, The precipitation behavior of an Al-Cu-Mg-Ag alloy under ECAP, Mater. Sci. Eng. A. 588 (2013) 65–75. https://doi.org/10.1016/j.msea.2013.09.021.

[41]   R.W.K. Honeycombe, The plastic deformation of metals, 2nd ed., Hodder Arnold, New York, 1984.

[42]   B.. Li, F.. Wawner, Dislocation interaction with semicoherent precipitates (Ω phase) in deformed Al–Cu–Mg–Ag alloy, Acta Mater. 46 (1998) 5483–5490. https://doi.org/10.1016/S1359-6454(98)00188-8.

[43]   S. Bai, H. Di, Z. Liu, Dislocation interaction with Ω phase in crept Al-Cu-Mg-Ag alloys, Mater. Sci. Eng. A. 651 (2016) 399–405. https://doi.org/10.1016/j.msea.2015.10.031.

[44]   M. Gazizov, R. Kaibyshev, Effect of over-aging on the microstructural evolution in an Al-Cu-Mg-Ag alloy during ECAP at 300° C, J. Alloys Compd. 527 (2012) 163–175. https://doi.org/10.1016/j.jallcom.2012.02.144.

[45]   M. Gazizov, C.D. Marioara, J. Friis, S. Wenner, R. Holmestad, R. Kaibyshev, Precipitation behavior in an Al–Cu–Mg–Si alloy during ageing, Mater. Sci. Eng. A. (2019) 138369. https://doi.org/10.1016/J.MSEA.2019.138369.